Nano Research 2015, 8(7): 2340–2350
DOI 10.1007/s12274-015-0744-8
Research Article
ISSN 1998-0124
CN 11-5974/O4

Field-effect transistor with a chemically synthesized MoS_2 sensing channel for label-free and highly sensitive electrical detection of DNA hybridization

Doo-Won Lee[1,§], Jinhwan Lee[2,§], Il Yung Sohn[1], Bo-Yeong Kim[3], Young Min Son[4], Hunyoung Bark[3], Jaehyuck Jung[3], Minseok Choi[5], Tae Hyeong Kim[5], Changgu Lee[2,3] (✉), and Nae-Eung Lee[1,3,4] (✉)

[1] *Department of Advanced Materials Science & Engineering, Sungkyunkwan University, Suwon, Gyunggi-do 440-746, Republic of Korea*
[2] *Department of Mechanical Engineering, Sungkyunkwan University, Suwon, Gyunggi-do 440-746, Republic of Korea*
[3] *SKKU Advanced Institute of Nanotechnology (SAINT), Sungkyunkwan University, Suwon, Gyunggi-do 440-746, Republic of Korea*
[4] *Samsung Advanced Institute for Health Sciences & Technology (SAIHST), Sungkyunkwan University, Suwon, Gyeonggi-do 440-746, Republic of Korea*
[5] *New Materials Team, Future Device R&D Department, LG Electronics Advanced Research Institute, Seoul 137-724, Republic of Korea*
[§] *These authors contributed equally to this work.*

Received: 16 December 2014
Revised: 3 February 2015
Accepted: 10 February 2015

KEYWORDS
two-dimensional(2D) materials, MoS_2, field-effect transistor, biosensor, deoxyribonucleic acid (DNA) hybridization

ABSTRACT

A field-effect transistor (FET) with two-dimensional (2D) few-layer MoS_2 as a sensing-channel material was investigated for label-free electrical detection of the hybridization of deoxyribonucleic acid (DNA) molecules. The high-quality MoS_2-channel pattern was selectively formedthrough the chemical reaction of the Mo layer with H_2S gas. The MoS_2 FET was very stable in an electrolyte and inert to pH changes due to the lack of oxygen-containing functionalities on the MoS_2 surface. Hybridization of single-stranded target DNA molecules with single-stranded probe DNA molecules physically adsorbed on the MoS_2 channel resulted in a shift of the threshold voltage (V_{th}) in the negative direction and an increase in the drain current. The negative shift in V_{th} is attributed to electrostatic gating effects induced by the detachment of negatively charged probe DNA molecules from the channel surface after hybridization. A detection limit of 10 fM, high sensitivity of 17 mV/dec, and high dynamic range of 10^6 were achieved. The results showed that a bio-FET with an ultrathin 2D MoS_2 channel can be used to detect very small concentrations of target DNA molecules specifically hybridized with the probe DNA molecules.

1 Introduction

Label-free electrical detection of biomolecules with a bioelectronic field-effect transistor (bio-FET) transducer utilizing nanoscale materials responsive to biomolecular interactions has been extensively investigated

Address correspondence to Nae-Eung Lee, nelee@skku.edu;Changgu Lee, peterlee@skku.edu

owing to its high sensitivity and low limit of detection (LOD) [1, 2]. Bio-FETs with one-dimensional (1D) Si nanowires (Si-NWs) [3, 4] or carbon nanotubes (CNTs) [5, 6] have shown effective detection of cancer biomarkers down to the femtomolar (fM) range in human serum. However, the low-cost, scalable, and reliable fabrication of bio-FETs utilizing 1D nanostructures is still limited because of the constraints of nanofabrication [5–7]. In the past few years, nanoelectronic devices based on two-dimensional (2D) nanomaterials have attracted great attention owing to their many interesting electrical, optical, and mechanical properties [8–16]. Because the 2D nature of bio-FETs provides a large sensing area for high responsivity [17], ease of fabrication compared to 1D nanobiosensors [18, 19], low noise level in solution [20–22], and high sensitivity to biomolecules [23–25], bio-FETs based on 2D graphene (Gr) [12–14, 23, 26] or reduced grapheme oxide (rGO) [12, 14, 18, 19, 24, 27, 28], have been extensively studied for the electrical detection of protein [14, 18, 19, 24, 29, 30] and deoxyribonucleic acid (DNA) molecules [31–34]. These FETs were shown to have the capability of detecting as little as 10 pM of target DNA using DNA-probe molecules conjugated with Au nanoparticles on chemical-vapor-deposited (CVD) Gr [31]. A 1-pM detection limit was achieved on pristine CVD Gr transferred using a gold layer [32]. Furthermore, a low limit of detection with a 1-fM range of target proteins was reported using an rGO FET fabricated via self-assembly methods [18].

Another interesting 2D nanomaterial candidate for bio-FETs as a channel is single-layer or few-layer MoS_2. Unlike ambipolar Gr, however, single-layer MoS_2 is typically an n-type semiconductor with a direct band gap of 1.8 eV. Developing new applications based on single- or few-layer MoS_2 is of great interest in various fields. Recently, diverse applications of MoS_2 including transistors [35–42] and sensor devices [43–48] have been investigated. FETs using single-layer MoS_2 exfoliated mechanically from bulk MoS_2 showed excellent electrical properties such as high current on/off ratios (10^8), low subthreshold swing, and high mobility at room temperature [35]. Optical [36], chemical [43, 44], and biological [45, 46] sensors utilizing the responses of MoS_2 to various stimuli have been reported.

Bio-FETs with a mechanicallyexfoliated 2D MoS_2 semiconductor channel and an oxide gate dielectric layer showed great promise for label-free electrical detection of biomolecular interactions [45]. The reported potentiometric bio-FET demonstrated the detection of biotin–streptavidin interactions at concentrations as low as 100 fM. Furthermore, an ultra-thin HfO_2 gate dielectric layer on a MoS_2 channel was usedbecause of the difficulty in immobilizing the probe proteins directly on the MoS_2 surface. High-quality MoS_2 films do not possess dangling bonds or π electrons for covalent attachment of linker or probe molecules. The bio-FET also demonstrated improved protein-detection sensitivity compared to a solution-gated Gr FET with an oxide gate dielectric, which is attributed to the existence of a band gap in MoS_2. The detection of PSA antigen at concentrations as low as 375 fM using a PSA antibody immobilized on a HfO_2 dielectric layer deposited on a mechanically-exfoliated MoS_2 channel in a solution-gated FET configuration was also reported previously [46]. Because of the limits of fabrication of bio-FETs using mechanically exfoliated MoS_2, which requires e-beam lithography, developing a facile fabrication method for bio-FETs based on chemically synthesized MoS_2 is expected to extend the applicability of bio-FETs based on 2D MoS_2. Large-area, ultrathin MoS_2 films that can be synthesized more readily through chemical synthesis methods will be more practical for label-free electrical detection of biomolecules using MoS_2 bio-FETs. The direct attachment of probe biomolecules on the MoS_2-channel surface also provides more effective detection in the FET structure because of the direct coupling of biomolecular charges with the 2D semiconductor channel within the electrochemical double layer (EDL). Furthermore, there have been no previous reports on the detection of DNA hybridization using MoS_2 bio-FETs.

Herein, we demonstrate a label-free, highly sensitive, and scalable electrical biosensor for detecting DNA hybridization using bio-FETs with the 2D MoS_2 channel directly functionalized by single-stranded DNA probe molecules. Multiple MoS_2-channel patterns were selectively synthesized through the chemical reaction of H_2S gas with an ultrathin Mo layer having the channel pattern. DNA probe molecules could be directly immobilized on the MoS_2 surface through van der Waals interactions [49], which enables the

detection of hybridization between the probe and target DNA molecules. The results showed that the hybridization of single-stranded target DNA with single-stranded complementary probe DNA molecules led to the detachment of hybridized double-stranded conjugates and, consequently, changes in the threshold voltage (V_{th}) and the conductivity of the channel in the transfer characteristics. Target DNA molecules of concentrations as low as 10 fM could be detected in the MoS_2 bio-FET with a high sensitivity of 17 mV/dec in the shift of V_{th} and a dynamic range of 10^6.

2 Results and discussion

Multiple four-layer MoS_2 FETs were fabricated simultaneously on a silicon wafer, and a polydimethylsiloxane (PDMS) well containing the MoS_2 FETs was formed on the substrate to hold the analyte solutions (Fig. 1(a)). A schematic of the device structure is shown in Fig. 1(b). Optical images of six MoS_2 FETs with the PDMS well and a single MoS_2 FET device are shown in Figs. 1(c) and 1(d), respectively. MoS_2 FETs are fabricated on the heavily p-doped Si wafer with a SiO_2 (300 nm) layer so that the FETs can be characterized in both the back-gated (i.e., bottom-gated) configuration with the heavily p-doped layer as a gate electrode and the SiO_2 layer as a gate dielectric material as well as in the solution-gated (i.e. top-gated) configuration with the EDL in the electrolyte as a gate dielectric and the Ag/AgCl reference electrode as a gate electrode. For the fabrication of MoS_2 FETs, the pattern of the MoS_2 channel was first formed through a selective chemical reaction of H_2S gas with the channel pattern of an ultrathin Mo layer on the Si/SiO_2 substrate. Details of the chemical synthesis process to form the MoS_2-channel pattern are presented in the Experimental Section, and the fabrication-process sequence is shown in Fig. S1 (in the Electronic Supplementary Material (ESM)). An important feature of the device fabrication is to passivate the source–drain electrodes from the electrolyte in order to minimize the leakage between the source–drain electrodes and the reference electrode during solution-gated measurements. For this purpose, a negative photoresist pattern, SU-8, was formed (see the details in Experimental Section).

Fundamental properties of the ultra-thin MoS_2 layer formed via a chemical synthesis method were investigated using X-ray photoelectron spectroscopy (XPS), Raman spectroscopy, and atomic force microscopy (AFM). The chemical binding states of the MoS_2 film were investigated by measuring the binding energies of Mo and S orbitals using XPS. In Fig. 2(a), the detailed binding energy profile for Mo 3d spectra shows three peaks at 232.59, 299.44, and 226.64 eV,

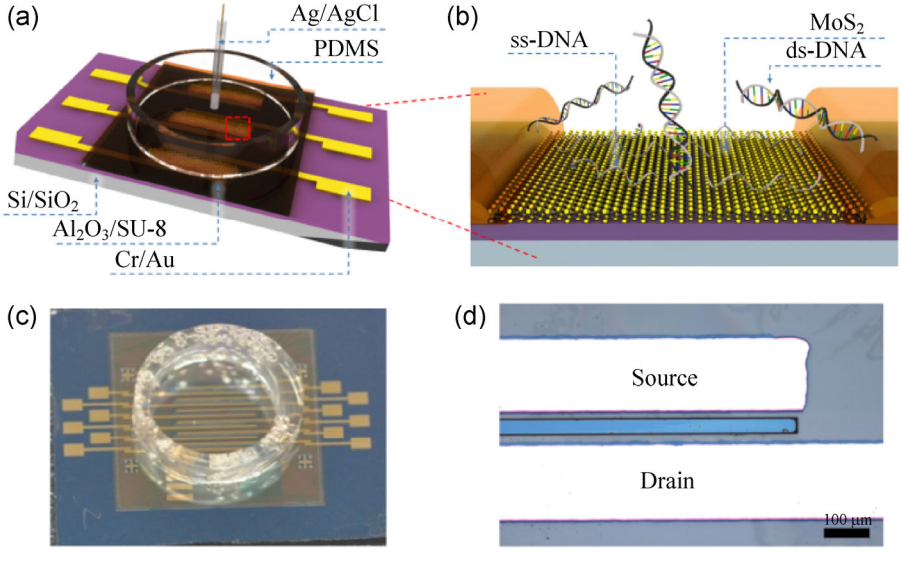

Figure 1 (a) Configuration of back-gated and solution-gated FETs on Si/SiO_2 substrate, (b) schematic of MoS_2 FET, (c) optical image of six MoS_2 FETs, and (d) optical image of a single device composed of the MoS_2 channel.

corresponding to Mo $3d_{3/2}$, Mo $3d_{5/2}$, and S 2p orbitals, respectively. S $2p_{1/2}$ and S $2p_{3/2}$ orbitals are observed at 163.49 and 162.29 eV, respectively. These peaks are consistent with the typical spectra of the MoS_2 layer reported previously [50]. Figure 2(b) shows the Raman spectra collected from as-grown and mechanically exfoliated pristine MoS_2. The Raman modes, E_{2g} and A_{1g} related to interlayer bonding and lattice vibrations, were observed at 382.6 and 406.6 cm^{-1}, respectively. The frequency difference between these two modes can be used to determine the number of layers and the thickness of single- and few-layer MoS_2 [51].

The Raman spectrum of the chemicallysynthesized MoS_2 film in this work was similar to that of mechanically exfoliated MoS_2 with four layers. The MoS_2 synthesized here would therefore be of 4 layers. Additionally, the thickness uniformity was measured via Raman mapping in Fig. 2(c). The color distribution in the mapped image demonstrates that synthesized MoS_2 has good uniformity with a frequency difference of ~24 cm^{-1} over the entire area.

Moreover, the thickness and roughness were measured using AFM for comparison with the results of Raman spectroscopy. Figure 2(d) shows the topology of the patterned MoS_2 channel and cross-sectional line profile of its edge. The thickness was 2.65 nm, which is in agreement with thickness of 4 layers, and the root mean square (RMS) roughness was 0.31 nm (see Fig. S2 in the ESM). These results are consistent with the results of Raman mapping in Fig. 2(c).

In order to investigate the electrical characteristics of back-gated MoS_2 FETs using a SiO_2 gate dielectric layer on the Si substrate, the drain current (I_{DS}) was monitored before measuring the device properties of the MoS_2 solution-gated FETs by applying a back-gate bias voltage ($V_{G,back}$) to the silicon substrate as a back-gate electrode beneath the SiO_2 gate dielectric. Output characteristics of the back-gated FET with the four-layer MoS_2 channel were obtained by applying a source–drain voltage (V_{DS}) up to 50 V for $V_{G,back}$ ranging from 0 to 80 V with intervals of 20 V (Fig. S3(a) in the ESM). The device was turned on by the electrons

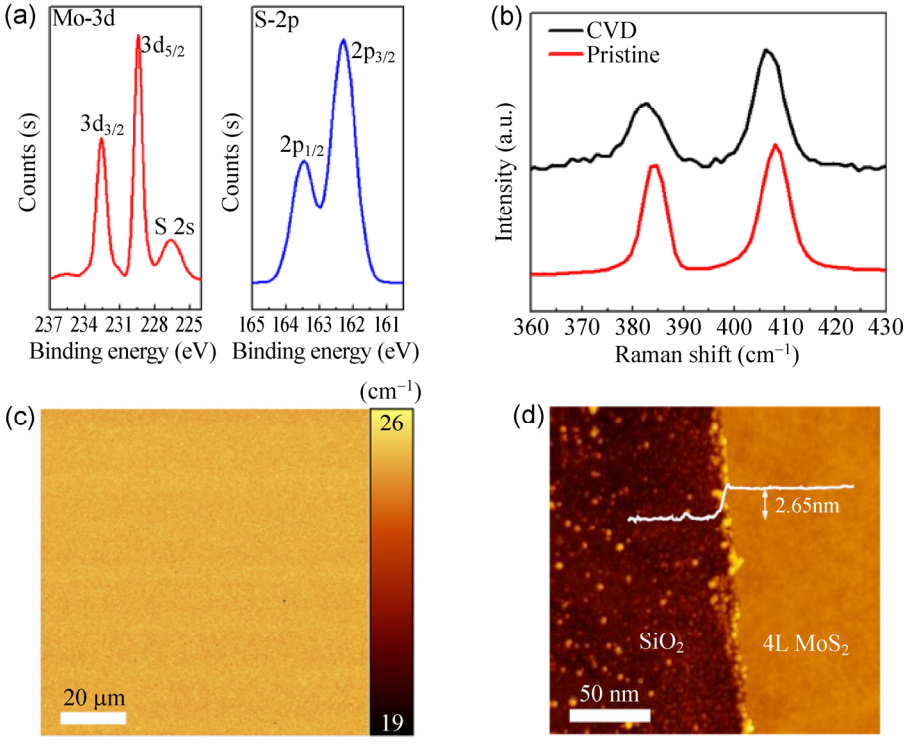

Figure 2 (a) Spectra of binding energies in Mo 3d and S 2p orbitals, (b) Raman spectra of pristine- and CVD-MoS_2, (c) Raman mapping image of the difference between E_{2g} and A_{1g} modes,and (d) topological image of the patterned MoS_2 channel. The thickness of MoS_2 is 2.65 nm, as determined from the cross-sectional line profile.

accumulated in the n-type MoS_2 channel under a positive $V_{G,back}$ applied by the gate electrode. Transfer characteristics of back-gated MoS_2 FETs with a biasing $V_{G,back}$ up to 100 V at a V_{DS} of 10 V were also measured. By analyzing the transfer characteristics (Fig. S3(b) in the ESM), the field-effect channel mobility (μ) and V_{th} values were estimated to be 0.019 $cm^2/(V{\cdot}s)$ and 31.7 V, respectively. The current on/off ratio was 10^2. The V_{th} value is large because of the low gate capacitance of the SiO_2 gate dielectric layer, which is quite thick in the back-gated configuration.

The transfer characteristics of a solution-gated FET with a four-layered MoS_2 channel in an electrolyte (PBS solution, 0.1x) werealso measured using $V_{G,top}$ from 0 to 1 V at a V_{DS} of 0.1 V (Fig. 3(a)). As previously mentioned, the source–drain electrodes of the devices were encapsulated using SU-8 epoxy to minimize the effects of leakage current and adsorption of biomolecules on the electrodes during the detection of biomolecular interactions. The current on/off ratio was increased to 10^5, and the V_{th} was reduced to 0.76 V because of the high gate capacitance of EDL (~29 $\mu F/cm^2$) with a very low thickness of ~2.4 nm in the PBS (0.1x) solution. The μ value was increased to 4.11 $cm^2/(V{\cdot}s)$. Since the devices show good electrical characteristics, the stability of the as-fabricated devices was investigated.

The electrical stability of the MoS_2 FET was investigated by measuring the electrical properties of the fabricated devices as a function of time in the PBS solution. In particular, the long-term stability of device characteristics is very important for the electrical detection of DNA hybridization because of the long time required for DNA hybridization. It was found

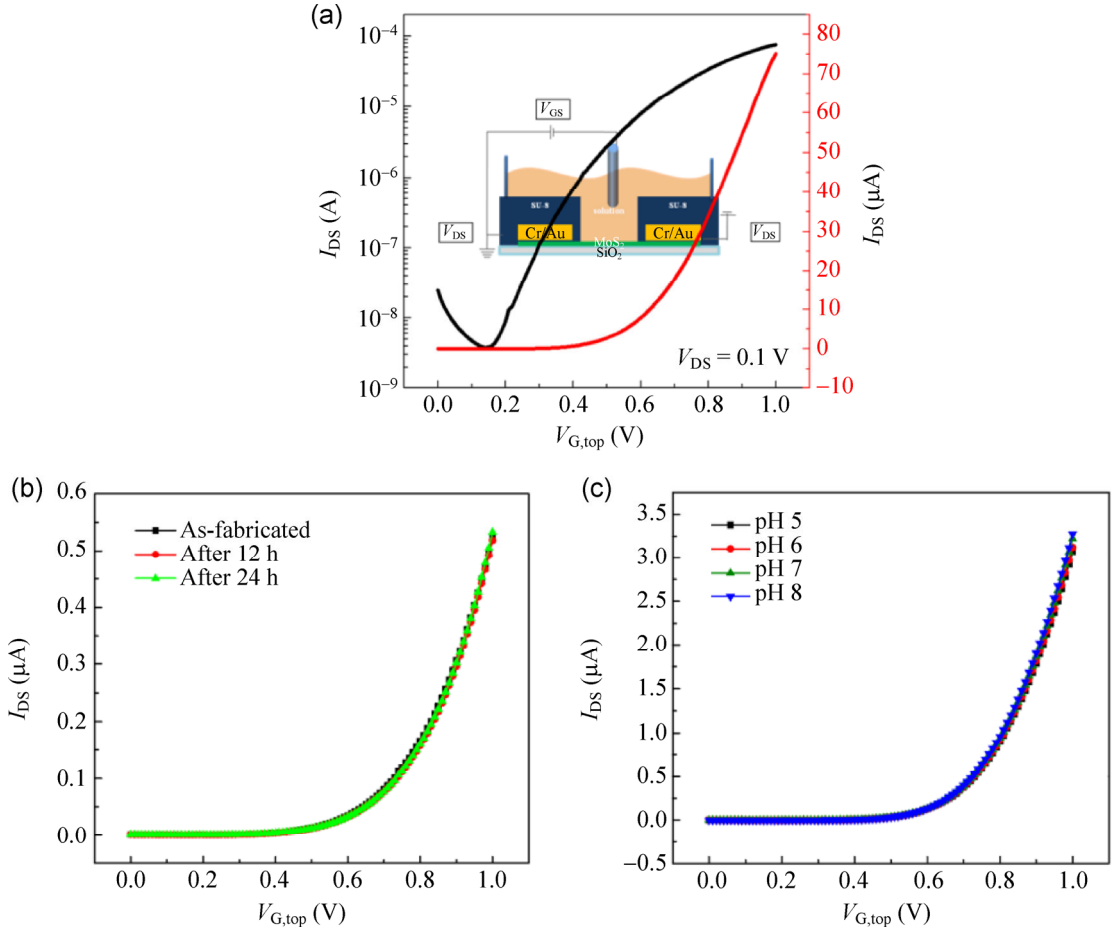

Figure 3 (a) Transfer characteristics of solution-gate MoS_2 FET measured at V_{DS} = 0.1 V; (b) transfer characteristics of solution-gated MoS_2 FET in PBS (0.1x) solution (pH = 7.4) measured with respect to time at V_{DS} = 0.1 V; and (c) transfer characteristics of solution-gated MoS_2 FET in the PB solutions with different pH values at V_{DS} = 0.1 V.

that the transfer characteristics and V_{th} values of the MoS_2 FET in electrolyte were stable when the devices were measured after 12 and 24 h in the PBS solution (Fig. 3(b)).

Transfer characteristics of MoS_2 FETs in phosphate buffer (PB) solutions with varying pH values from 5 to 8 were measured in order to evaluate the effects of pH values on the solutiongating of the FETs. The results in Fig. 3(c) show no significant changes in transfer characteristics and V_{th} values, which indicate the inertness of the MoS_2-channel layer to H^+ ions. For pH responsivity of the sensing materials in bio-FETs, electrostatic gating effects should occur when H^+ ions interact with the surface functionality of neutral OH on the surface of sensing materials through protonation ($–OH + H^+ = –OH^{2+}$) and deprotonation ($–OH = –O^- + H^+$); these reactions result in a net increase of positive or negative charges on the surface [52]. No V_{th} shift was observed, indicating that the MoS_2 surface is inert and that no oxygen-containing functionalities exist on the surface.

Time-dependent measurements of the pH responsivity of MoS_2 FETs were performed by adding PB solutions with different pH values to the PDMS well. The results indicate the electrical stability of the device under repetitive gate biasing for 600 s with no changes in the I_{DS} (Fig. S4(a) in the ESM). When PB solutions of different pH values were added repetitively, there was a spike in I_{DS}, presumably due to perturbation in the solution, but its value subsequently saturated to the similar I_{DS} (Fig. S4(b) in the ESM). When PB solutions of pH increasing from 5 to 6 and to 7 (Fig. S4(c) in the ESM) and PB solutions of pH decreasing from 8 to 7 and to 6 (Fig. S4(d) in the ESM)) were added, the final I_{DS} value did not change significantly.

The effect of different ionic concentrations of PBS solutions on the transfer characteristics was investigated. An increase in PBS concentration causes a decrease in EDL thickness, which results in a positive shift of V_{th} due to reduced gate capacitance. As shown in Fig. S5 (in the ESM), V_{th} values were 0.77, 0.82, and 0.84 V for PBS solutions of concentrations 0.01x, 0.1x, and 1x, respectively. Furthermore, reducing the gate capacitance by increasing the PBS concentration led to a decrease in I_{DS}. Electrical measurements of the hybridization of target DNA with the probe DNA molecules were performed for the FET with a four-layer MoS_2 channel in the electrolyte. As mentioned previously, the lack of dangling bonds on the MoS_2 basal plane makes the immobilization of probe DNA molecules through covalent bonding or other strong bonds difficult. However, nucleobases of probe DNA molecules can interact with the basal plane of MoS_2 through van der Waals forces [49]. For example, the physical adsorption of aromatic and conjugated compounds on the basal plane of MoS_2 was demonstrated theoretically and experimentally [53, 54]. When the probe DNA molecules were immobilized on the basal plane of the MoS_2 channel, the transfer characteristics of the device changed significantly. The I_{DS} was significantly reduced at V_{DS} = 0.1 V, and V_{th} was shifted in the positive direction (Fig. 4(a)). The probe DNA molecules physically adsorbed on the basal plane of MoS_2 are negatively charged because of their phosphate backbone. The negative charges of the adsorbed probe DNAs on the n-type MoS_2 channel reduce the effective positive gate field applied through the reference electrode and, consequently, reduce the density of the accumulated electrons. This, in turn, reduces the I_{DS} and induces the shift in V_{th} in the positive direction.

Measurements of the transfer characteristics of DNA hybridization were performed by adding complementary target DNA molecules in the PDMS well on the FET functionalized with the probe DNA. The transfer characteristics during measurements were obtained by applying $V_{G,top}$ from 0 to 1 V at a V_{DS} of 0.1 V. When the complementary target DNA with a concentration ranging from 10 fM to 100 nM was added and hybridized with the probe DNA molecules, the I_{DS} increased and V_{th} shifted in the negative direction, i.e., closer to the transfer curve of pristine MoS_2 FET (Fig. 4(a)). The results indicate the reduction of negative biomolecular changes on the MoS_2 channel. However, when non-complementary and single-base mismatched DNA molecules with a concentration ranging from 10 fM to 10 nM were added, the I_{DS} and V_{th} values did not vary significantly (Figs. 4(b) and 4(c), respectively). The LOD value obtained here in the fM range is larger than the LODs in the pM range obtained from CVD Gr FETs [31, 32]. The results indicate that the probe DNA molecules on the MoS_2 channel are intact because of a lack of interaction

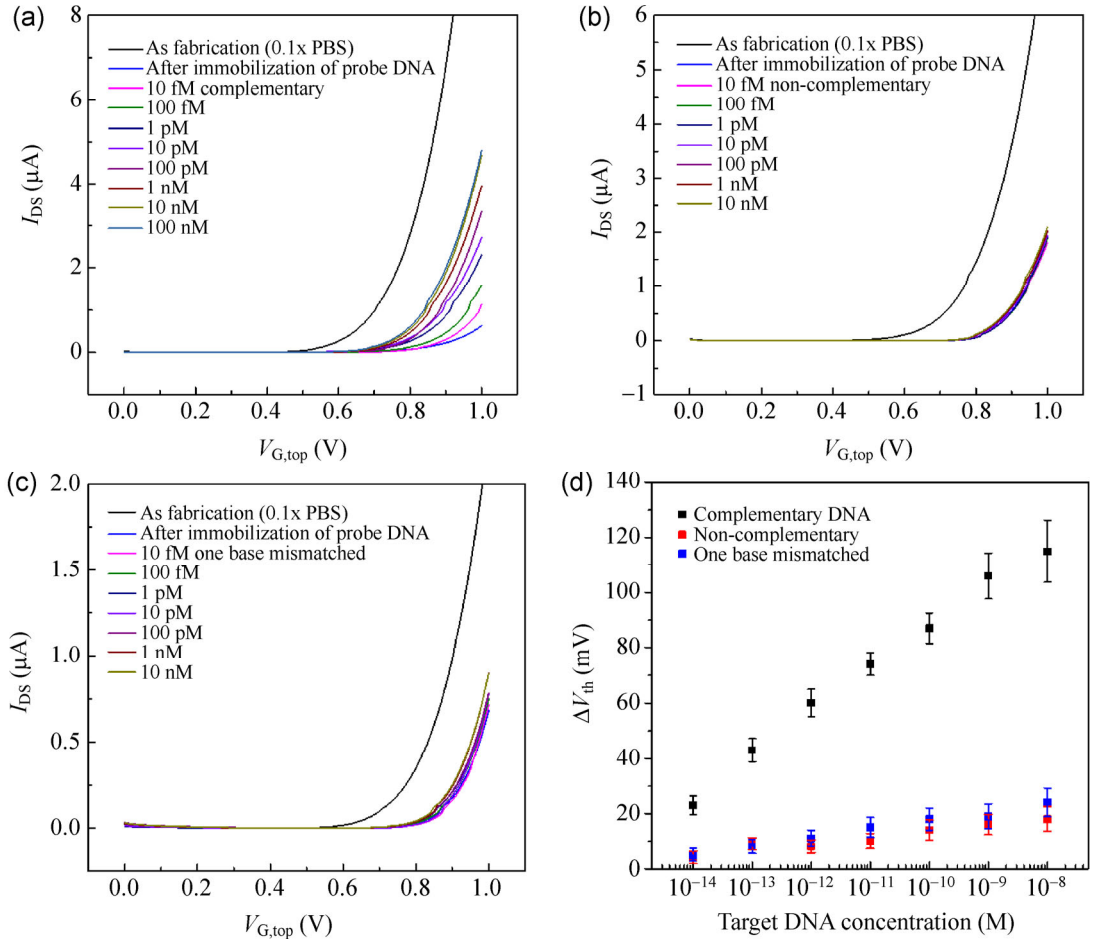

Figure 4 Transfer characteristics of MoS_2 FETs immobilized with the probe DNA molecules and hybridized with (a) complementary, (b) non-complementary, and(c) single-base mismatched DNA molecules with a concentration ranging from 10 fM to 10 nM, (d) shifts in the threshold voltage (ΔV_{th}) as a function of the concentration of complementary, non-complementary and single-base mismatched DNA molecules. Each ΔV_{th} value was obtained by averaging the data from the transfer characteristics of three devices, and a ΔV_{th} of 17 meV/dec in the negative direction was observed.

of non-complementary and single-base mismatched DNA molecules with the probe DNA.

The shifts in V_{th} in Fig. 4(a) were plotted as a function of target DNA concentration by averaging the data from three devices. The averaged sensitivity of DNA hybridization in the MoS_2 FET was found to be 17 mV/dec (Fig. 4(d)). A large dynamic range of 10^6 was obtained. When the non-complementary and single-base mismatched DNA molecules were added, the shift in the V_{th} was negligible, as shown in Fig. 4(d). The data in Fig. 4(d) indicate that the hybridization of complementary target DNA molecules with probe DNA molecules effectively caused a shift in the V_{th}; thus, the V_{th} shift can be used as a sensing parameter. Furthermore, the I_D and μ values increased as the target DNA concentration increased.

The sensing mechanism can be deduced from the experimental data in Fig. 4. Negative charges of the probe DNA molecules adsorbed on the MoS_2 channel caused the V_{th} to shift in the positive direction. These effects can be explained by the electrostatic gating effects, in which the negative charges on the n-type MoS_2 channel reduce the effective gate field under a positive gate biasing condition and, in turn, shift V_{th} in the positive direction for the n-type channel. However, with the addition of complementary target DNA molecules, the shift of V_{th} in the negative direction indicates the reduction of negative charges, which is attributed to the desorption of hybridized, double-stranded DNA conjugates from the MoS_2 channel due

to their decreased binding force and increased effective gate field (see Fig. S6 in the ESM). The results are consistent with the reports that hybridized, double-stranded DNA conjugatesformed by binding target DNA molecules with probe DNA molecules bound non-covalently to MoS_2 [49] and Gr [55–57]. An increase in I_{DS} at a given $V_{G,top}$ is attributed to electrostatic gating effects resulting in the increase in electron density in the channel and increased μ at a given $V_{G,top}$. The increase in the μ value is presumably due to a reduction in charge scattering due to desorption of the target DNA from the MoS_2-channel surface. Since non-complementary target DNA molecules do not cause the detachment of probe DNA molecules from the surface, a shift in V_{th} did not occur.

3 Conclusions

A MoS_2 bio-FET was successfully fabricated for the sensitive detection of DNA hybridization. The MoS_2 channel was formed through selective chemical synthesis that facilitates the fabrication process and provides a large sensing area. The target DNA molecules were directly immobilized on the MoS_2 surface, instead of using a gate oxide layer between the MoS_2 and electrolyte for improved coupling of surface charges with the channel conductance. The results indicate that the MoS_2 bio-FETs can be used to detect target DNA molecules with a low detection limit of 10 fM, high dynamic range of 10^6, and high sensitivity of 17 mV/dec in the shift of V_{th}. It was found that hybridized DNA conjugates are detached from the MoS_2 channel and electrostatic gating effects because of the change in the surface charge density of the channel, which contributes to the V_{th} shift and the change in the drain current. This label-free, highly sensitive, and scalable MoS_2 bio-FET can be operated at a very low voltage with low power consumption and has great potential in many applications such as disease diagnostics, environmental monitoring, food safety, and public security based on the detection of DNA molecules. In addition to the promising results of this work, further research on the reusability of the MoS_2 DNA sensor and the effects of MoS_2 layers on the sensitivity need to be performed for the advancement of MoS_2 bio-FET devices in the biosensing field.

4 Method

4.1 Materials synthesis

An ultrathin MoS_2 film was used as a sensing layer for detecting DNA hybridization and as an active channel in a solution-gated FET structure. The Si/SiO_2 (300 nm) wafer was heated in a mixture of NH_4OH:H_2O_2:deionized (DI) water (1:1:5) at 85 ˚C for 30 min. The SiO_2 layer can be used as a gate dielectric layer during back-gated measurements. MoS_2 films were synthesized through the direct sulfurization of Mo metal on the substrate. The synthesis of patterned MoS_2 begins with the deposition of a 1-nm-thick Mo metal pattern of the channel on a SiO_2/Si wafer at ~0.1 Å/s through e-beam evaporation using a shadow mask. The Mo pattern on the substrate was heated up to 750 ˚C within a few seconds under Ar gas flow at a rate of 50 standard cubic centimeters per minute (sccm) in a quartz chamber. After the pre-annealing process, the H_2S:H_2:Ar (1:5:50) reaction gas mixture was injected for 15 min to synthesize MoS_2. The chamber pressure was maintained at 0.31 Torr during the synthesis step. The surface morphology of MoS_2 was studied using atomic force microscopy (NanoWizard 3, JPK Instruments, Germany). Raman spectroscopy (Alpha 300 M, WITec, Germany) was used to check the quality of the formed MoS_2 film. XPS(VG ESCALAB 210, Thermo Scientific) was used to investigate the chemical binding states of the MoS_2 film.

4.2 Device fabrication and measurements

Prior to the FET fabrication, the MoS_2 film was annealed to remove residues in an Ar atmosphere at 350 ˚C for 9 h. Subsequently, Au/Cr drain–source electrodes (60 nm/10 nm) were formed on the patterned MoS_2 using a shadow mask and thermal evaporator. The channel length (L) and width (W) of the MoS_2 FET were 300 and 6,000 μm, respectively, with a W/L ratio of 20. The fabricated device was annealed in an Ar atmosphere for 4 h. A critical step is to isolate the source–drain electrodes from the electrolytes to block the leakage current through the electrolytes by forming the encapsulation layer. For this purpose, an SU-8 pattern was formed via photolithography after the deposition of an Al_2O_3 layer with a thickness of 10 nm

on the entire surface of the wafer after the formation of source–drain electrodes on the MoS_2 channel. Here, the Al_2O_3 layer acts as a buffer layer protecting the MoS_2 layer during the photolithography of the SU-8 pattern and improves the adhesion of SU-8 on the MoS_2 surface. Subsequently, the Al_2O_3 layer on the sensing area of the MoS_2 channel was etched using a H_3PO_4:water (1:1) solution for 3 min. Finally, the well was formed using PDMS (Sylgard 184) cured at 80 ℃ for measurements of DNA hybridization.

For the electrical characterization of the as-fabricated devices, transfer characteristics were measured by biasing the gate voltage ($V_{G,back}$) with a back-gate configuration, and these were compared with those of solution-gated measurements of the MoS_2 FET using a Ag/AgCl reference electrode. Three types of single-stranded DNA molecules of the probe DNA (5′-CTG TCT TGA ACA TGA GTT-3′), complementary target DNA (5′-AAC TCA TGT TCA AGA CAG-3′), and non-complementary (5′-GGT CTG CAC CTG GAG TGA-3′) and single-base mismatched (5′-AAC TCA TGA TCA AGA CAG-3′) DNA molecules (M-biotech Co., Republic of Korea) were synthesized and used for sensing experiments. The solutions of probe DNA, complementary DNA, and non-complementary DNA molecules were prepared by diluting them in PBS (0.1x) solution. The probe DNA molecule solutions with a concentration of 10 μM were prepared through dilution in PBS (0.1x) solution and subsequent soaking in PDMS well with MoS_2 FET for 16 h for immobilization. Subsequently, a rinsing process with fresh PBS solutions was followed in order to remove weakly bound DNAs. The electrical measurements of DNA hybridization in the solution-gated MoS_2 FET with the PDMS well and PBS solutions containing different concentrations of the target DNA molecules were performed by biasing the $V_{G,top}$ using a Ag/AgCl reference electrode.

Acknowledgements

This research was supported by the Basic Science Research Program (Nos. 2009-0083540 and 2013R1A2A1A01015232) through the National Research Foundation (NRF) funded by the Ministry of Science, ICT & Future Planning.

Electronic Supplementary Material: Supplementary material (fabrication process of the MoS_2 FET, surface morphology of the patterned MoS_2 channel, characteristics of the back-gated MoS_2 FET, and schematic illustration of the sensing mechanism) is available in the online version of this article at http://dx.doi.org/10.1007/s12274-015-0744-8.

References

[1] Bellan, L. M.; Wu, D.; Langer, R. S. Current trends in nanobiosensor technology. *Wiley Interdiscip. Rev. Nanomed. Nanobiotechnol*. **2011**, *3*, 229–246.

[2] Kirsch, J.; Siltanen, C.; Zhou, Q.; Revzin, A.; Simonian, A. Biosensor technology: Recent advances in threat agent detection and medicine. *Chem. Soc. Rev.* **2013**, *42*, 8733–8768.

[3] Timko, B. P.; Cohen-Karni, T.; Quan, Q.; Tian, B. Z.; Lieber, C. M. Design and implementation of functional nanoelectronic interfaces with biomolecules, cells, and tissue using nanowire device arrays. *IEEE Trans. Nanotechnol.* **2010**, *9*, 269–280.

[4] Zheng, G. F.; Patolsky, F.; Cui, Y.; Wang, W. U.; Lieber, C. M. Multiplexed electrical detection of cancer markers with nanowire sensor arrays. *Nat. Biotechnol.* **2005**, *23*, 1294–1301.

[5] Ray, S.; Chandra, H.; Srivastava, S. Nanotechniques in proteomics: Current status, promises and challenges. *Biosens. Bioelectron.* **2010**, *25*, 2389–2401.

[6] Vashist, S. K.; Zheng, D.; Al-Rubeaan, K.; Luong, J. H. T.; Sheu, F. S. Advances in carbon nanotube based electrochemical sensors for bioanalytical applications. *Biotechnol. Adv.* **2011**, *29*, 169–188.

[7] Jacobs, C. B.; Peairs, M. J.; Venton, B. J. Review: Carbon nanotube based electrochemical sensors for biomolecules. *Anal. Chim. Acta* **2010**, *662*, 105–127.

[8] Novoselov, K. S.; Geim, A. K.; Morozov, S. V.; Jiang, D.; Zhang, Y.; Dubonos, S. V.; Grigorieva, I. V.; Firsov, A. A. Electric field in atomically thin carbon films. *Science* **2004**, *306*, 666–669.

[9] Huang, X.; Yin, Z. Y.; Wu, S. X.; Qi, X. Y.; He, Q. Y.; Zhang, Q. C.; Yan, Q. Y.; Boey, F.; Zhang, H. Graphene-based materials: Synthesis, characterization, properties, and applications. *Small* **2011**, *7*, 1876–1902

[10] Wu, S. X.; He, Q. Y.; Tan, C. L.; Wang, Y. D.; Zhang, H. Graphene-based electrochemical sensors. *Small* **2013**, *9*, 1160–1172.

[11] Yuan, W. J.; Shi, G. Q. Graphene-based gas sensors. J. *Mater. Chem. A* **2013**, *1*, 10078−10091.

[12] Liu, S.; Guo, X. F. Carbon nanomaterials field-effect-transistor-based biosensors. *NPG Asia Mater.* **2012**, *4*, e23.
[13] Ohno, Y.; Maehashi, K.; Matsumoto, K. Chemical and biological sensing applications based on graphene field-effect transistors. *Biosens. Bioelectron.* **2010**, *26*, 1727–1730.
[14] Zhan, B. B.; Li, C.; Yang, J.; Jenkins, G.; Huang, W.; Dong, X. C. Graphene field-effect transistor and its application for electronic sensing. *Small* **2014**, *10*, 4042–4065.
[15] Buscema, M.; Steele, G. A.; van der Zant, H. S. J.; Castellanos-Gomez, A. The effect of the substrate on the raman and photoluminescence emission of single-layer MoS_2. *Nano Res.* **2014**, *7*, 561–571.
[16] Li, W. F.; Zhang, G.; Guo, M.; Zhang, Y. W. Strain-tunable electronic and transport properties of MoS_2 nanotubes. *Nano Res.* **2014**, *7*, 518–527.
[17] Cheng, Z. G.; Hou, J. F.; Zhou, Q. Y.; Li, T. Y.; Li, H. B.; Yang, L.; Jiang, K. L.; Wang, C.; Li, Y. C.; Fang, Y. Sensitivity limits and scaling of bioelectronic graphene transducers. *Nano Lett.* **2013**, *13*, 2902–2907.
[18] Kim, D. J.; Sohn, I. Y.; Jung, J. H.; Yoon, O. J.; Lee, N. E.; Park, J. S. Reduced graphene oxide field-effect transistor for label-free femtomolar protein detection. *Biosens. Bioelectron.* **2013**, *41*, 621–626.
[19] Kim, D. J.; Park, H. C.; Sohn, I. Y.; Jung, J. H.; Yoon, O. J.; Park, J. S.; Yoon, M. Y.; Lee, N. E. Electrical graphene aptasensor for ultra-sensitive detection of anthrax toxin with amplified signal transduction. *Small* **2013**, *9*, 3352–3360.
[20] Cheng, Z. G.; Li, Q.; Li, Z. J.; Zhou, Q. Y.; Fang, Y. Suspended graphene sensors with improved signal and reduced noise. *Nano Lett.* **2010**, *10*, 1864–1868.
[21] Heller, I.; Chatoor, S.; Männik, J.; Zevenbergen, M. A. G.; Dekker, C.; Lemay, S. G. Influence of electrolyte composition on liquid-gated carbon nanotube and graphene transistors. *J. Am. Chem. Soc.* **2010**, *132*, 17149–17156.
[22] Heller, I.; Chatoor, S.; Männik, J.; Zevenbergen, M. A. G.; Oostinga, J. B.; Morpurgo, A. F.; Dekker, C.; Lemay, S. G. Charge noise in graphene transistors. *Nano Lett.* **2010**, *10*, 1563–1567.
[23] Dong, X. C.; Shi, Y. M.; Huang, W.; Chen, P.; Li, L. J. Electrical detection of DNA hybridization with single-base specificity using transistors based on cvd-grown graphene sheets. *Adv. Mater.* **2010**, *22*, 1649–1653.
[24] He, Q. Y.; Sudibya, H. G.; Yin, Z. Y.; Wu, S. X.; Li, H.; Boey, F.; Huang, W.; Chen, P.; Zhang, H. Centimeter-long and large-scale micropatterns of reduced graphene oxide films: Fabrication and sensing applications. *ACS Nano* **2010**, *4*, 3201–3208.
[25] Ohno, Y.; Maehashi, K.; Yamashiro, Y.; Matsumoto, K. Electrolyte-gated graphene field-effect transistors for detecting pH and protein adsorption. *Nano Lett.* **2009**, *9*, 3318–3322.
[26] Huang, Y. X.; Dong, X. C.; Shi, Y. M.; Li, C. M.; Li, L. J.; Chen, P. Nanoelectronic biosensors based on CVD grown graphene. *Nanoscale* **2010**, *2*, 1485–1488.
[27] Pumera, M. Graphene in biosensing. *Mater. Today* **2011**, *14*, 308–315.
[28] Sohn, I. Y.; Kim, D. J.; Jung, J. H.; Yoon, O. J.; Nguyen Thanh, T.; Tran Quang, T.; Lee, N. E. pH sensing characteristics and biosensing application of solution-gated reduced graphene oxide field-effect transistors. *Biosens. Bioelectron.* **2013**, *45*, 70–76.
[29] Kim, J.; Yoon, M. Y. Recent advances in rapid and ultrasensitive biosensors for infectious agents: Lesson from bacillus anthracis diagnostic sensors. *Analyst.* **2010**, *135*, 1182–1190.
[30] Rao, S. S.; Mohan, K. V. K.; Atreya, C. D. Detection technologies for bacillus anthracis: Prospects and challenges. *J. Microbiol. Methods* **2010**, *82*, 1–10.
[31] Dong, X. C.; Shi, Y. M.; Huang, W.; Chen, P.; Li, L. J. Electrical detection of DNA hybridization with single-base specificity using transistors based on CVD-grown graphene sheets. *Adv. Mater.* **2010**, *22*, 1649–1653.
[32] Chen, T. Y.; Loan, P. T. K.; Hsu, C. L.; Lee, Y. H.; Wang, J. T. W.; Wei, K. H.; Lin, C. T.; Li, L. J. Label-free detection of DNA hybridization using transistors based on CVD grown graphene. *Biosens. Bioelectron.* **2013**, *41*, 103–109.
[33] Yin, Z. Y.; He, Q. Y.; Huang, X.; Zhang, J.; Wu, S. X.; Chen, P.; Lu, G.; Chen, P.; Zhang, Q. C.; Yan, Q. Y. et al. Real-time DNA detection using Pt nanoparticle-decorated reduced graphene oxide field-effect transistors. *Nanoscale* **2012**, *4*, 293–297.
[34] Lin, C. T.; Loan, P. T. K.; Chen, T. Y.; Liu, K. K.; Chen, C. H.; Wei, K. H.; Li, L. J. Label-free electrical detection of DNA hybridization on graphene using hall effect measurements: Revisiting the sensing mechanism. *Adv. Funct. Mater.* **2013**, *23*, 2301–2307.
[35] Radisavljevic, B.; Radenovic, A.; Brivio, J.; Giacometti, V.; Kis, A. Single-layer MoS_2 transistors. *Nat. Nanotechnol.* **2011**, *6*, 147–150.
[36] Yin, Z. Y.; Li, H.; Li, H.; Jiang, L.; Shi, Y. M.; Sun, Y. H.; Lu, G.; Zhang, Q.; Chen, X. C.; Zhang, H. Single-layer MoS_2 phototransistors. *ACS Nano* **2012**, *6*, 74–80.
[37] Yoon, Y.; Ganapathi, K.; Salahuddin, S. How good can monolayer MoS_2 transistors be? *Nano Lett.* **2011**, *11*, 3768–3773.
[38] Pu, J.; Yomogida, Y.; Liu, K. K.; Li, L. J.; Iwasa, Y.; Takenobu, T. Highly flexible MoS_2 thin-film transistors with ion gel dielectrics. *Nano Lett.* **2012**, *12*, 4013–4017.
[39] Zhang, Y. J.; Ye, J. T.; Matsuhashi, Y.; Iwasa, Y. Ambipolar MoS_2 thin flake transistors. *Nano Lett.* **2012**, *12*, 1136–1140.

[40] Li, H.; Wu, J.; Yin, Z. Y.; Zhang, H. Preparation and applications of mechanically exfoliated single-layer and multilayer MoS_2 and WSe_2 nanosheets. *Acc. Chem. Res.* **2014**, *47*, 1067–1075.

[41] Li, H.; Lu, G.; Yin, Z. Y.; He, Q. Y.; Li, H.; Zhang, Q.; Zhang, H. Optical identification of single- and few-layer MoS_2 sheets. *Small* **2012**, *8*, 682–686.

[42] Kwon, H.; Choi, W.; Lee, D.; Lee, Y.; Kwon, J.; Yoo, B.; Grigoropoulos, C. P.; Kim, S. Selective and localized laser annealing effect for high-performance flexible multilayer MoS_2 thin-film transistors. *Nano Res.* **2014**, *7*, 1137–1145.

[43] Li, H.; Yin, Z. Y.; He, Q. Y.; Li, H.; Huang, X.; Lu, G.; Fam, D. W. H.; Tok, A. I. Y.; Zhang, Q.; Zhang, H. Fabrication of single- and multilayer MoS_2 film-based field-effect transistors for sensing no at room temperature. *Small* **2012**, *8*, 63–67.

[44] He, Q. Y.; Zeng, Z. Y.; Yin, Z. Y.; Li, H.; Wu, S. X.; Huang, X.; Zhang, H. Fabrication of flexible MoS_2 thin-film transistor arrays for practical gas-sensing applications. *Small* **2012**, *8*, 2994–2999.

[45] Sarkar, D.; Liu, W.; Xie, X. J.; Anselmo, A. C.; Mitragotri, S.; Banerjee, K. MoS_2 field-effect transistor for next-generation label-free biosensors. *ACS Nano* **2014**, *8*, 3992–4003.

[46] Wang, L.; Wang, Y.; Wong, J. I.; Palacios, T.; Kong, J.; Yang, H. Y. Functionalized MoS_2 nanosheet-based field-effect biosensor for label-free sensitive detection of cancer marker proteins in solution. *Small* **2014**, *10*, 1101–1105.

[47] Wu, S. X.; Zeng, Z. Y.; He, Q. Y.; Wang, Z. J.; Wang, S. J.; Du, Y. P.; Yin, Z. Y.; Sun, X. P.; Chen, W.; Zhang, H. Electrochemically reduced single-layer MoS_2 nanosheets: Characterization, properties, and sensing applications. *Small* **2012**, *8*, 2264–2270.

[48] Zhang, Y.; Zheng, B.; Zhu, C. F.; Zhang, X.; Tan, C. L.; Li, H.; Chen, B.; Yang, J.; Chen, J. Z.; Huang, Y. et al. Single-layer transition metal dichalcogenide nanosheet-based nanosensors for rapid, sensitive, and multiplexed detection of DNA. *Adv. Mater.* **2015**, *27*, 935–939.

[49] Zhu, C. F.; Zeng, Z. Y.; Li, H.; Li, F.; Fan, C. H.; Zhang, H. Single-layer MoS_2-based nanoprobes for homogeneous detection of biomolecules. *J. Am. Chem. Soc.* **2013**, *135*, 5998–6001.

[50] Papageorgopoulos, C. A.; Jaegermann, W. Li intercalation across and along the van der Waals surfaces of MoS_2(0001). *Surf. Sci.* **1995**, *338*, 83–93.

[51] Lee, C.; Yan, H.; Brus, L. E.; Heinz, T. F.; Hone, J.; Ryu, S. Anomalous lattice vibrations of single- and few-layer MoS_2. *ACS Nano* **2010**, *4*, 2695–2700.

[52] Ang, P. K.; Chen, W.; Wee, A. T. S.; Loh, K. P. Solution-gated epitaxial graphene as pH sensor. *J. Am. Chem. Soc.* **2008**, *130*, 14392–14393.

[53] Moses, P. G.; Mortensen, J. J.; Lundqvist, B. I.; Nørskov, J. K. Density functional study of the adsorption and van der Waals binding of aromatic and conjugated compounds on the basal plane of MoS_2. *J. Chem. Phys.* **2009**, *130*, 104709.

[54] Heckl, W. M.; Smith, D. P.; Binnig, G.; Klagges, H.; Hänsch, T. W.; Maddocks, J. Two-dimensional ordering of the DNA base guanine observed by scanning tunneling microscopy. *Proc. Natl. Acad. Sci. USA* **1991**, *88*, 8003–8005.

[55] Lu, C. H.; Yang, H. H.; Zhu, C. L.; Chen, X.; Chen, G. N. A graphene platform for sensing biomolecules. *Angew. Chem. Int. Ed.* **2009**, *121*, 4879–4881.

[56] He, S. J.; Song, B.; Li, D.; Zhu, C. F.; Qi, W. P.; Wen, Y. Q.; Wang, L. H.; Song, S. P.; Fang, H. P.; Fan, C. H. A graphene nanoprobe for rapid, sensitive, and multicolor fluorescent DNA analysis. *Adv. Funct. Mater.* **2010**, *20*, 453–459.

[57] Bonanni, A.; Pumera, M. Graphene platform for hairpin-DNA-based impedimetric genosensing. *ACS Nano* **2011**, *5*, 2356–2361.